

## Phase Space Manipulation of Cold Free Radical OH Molecules

J. R. Bochinski, Eric R. Hudson, H. J. Lewandowski, Gerard Meijer,\* and Jun Ye<sup>†</sup>

*JILA, National Institute of Standards and Technology and Department of Physics,  
University of Colorado, Boulder, Colorado 80309-0440, USA*

(Received 7 June 2003; published 10 December 2003)

We report bunching, slowing, and acceleration of a supersonically cooled beam of diatomic hydroxyl radicals (OH). *In situ* observation of laser-induced fluorescence along the beam propagation path allows for detailed characterization of longitudinal phase-space manipulation of OH molecules through the Stark effect by precisely sequenced inhomogeneous electric fields.

DOI: 10.1103/PhysRevLett.91.243001

PACS numbers: 33.55.Be, 33.80.Ps, 39.10.+j

The advent of laser cooling and Bose-Einstein condensation has transformed atomic physics [1]. Molecules, with their richer internal structure, offer many new exciting research opportunities. Cold molecules can be used for novel collision studies, molecular optics and interferometry, quantum collective effects, quantum information science, long-range intermolecular states, precision spectroscopy and measurements, and investigations of chemistry in the ultracold regime. Presently, cold molecules are beginning to be produced and even confined within traps [2–4]. The revolutionary role played by cold atoms to the field of atomic physics may be duplicated by cold molecules to the field of physical chemistry and physical science overall.

The complex structure of molecular energy levels has so far precluded a straightforward implementation of laser cooling. Photo association [5] and Feshbach resonance association of cold atoms [6] represent effective approaches to the creation of cold diatomic molecules, but the techniques are limited to a small class of laser-cooled atoms. Molecules can also be cooled by thermalization with cryogenically refrigerated buffer gas, at a small cost of system complexity [3]. Working with molecules generated by supersonic expansion has a definite advantage: the internal—rotational and vibrational—degrees of freedom of the molecules are cooled and, primarily, only the ground state is populated. Furthermore, the translational temperature of the molecular beam is vastly reduced in its moving frame. Subsequently, the velocity of the molecules in the laboratory frame can be manipulated by an elegant method, which takes advantage of the Stark shift associated with polar molecules [7,8]; inhomogeneous pulsed electric fields controlled with a precise timing sequence may be used to selectively bunch, slow, or accelerate the molecules and accumulate them in a low temperature phase-space distribution.

In this Letter we demonstrate the feasibility of this approach for the diatomic hydroxyl radical (OH). The selection of the hydroxyl radical comes from both its extensive relevance to astrophysics [9] and physical chemistry [10] as well as its particular amenability to the Stark slowing technique. Recent theoretical studies

have also revealed particularly interesting prospects for study of cold collisions and controlled interactions between OH molecules [11]. These molecules possess permanent electric dipole moments that bring new opportunities for control over intermolecular interactions. When the translational energy becomes comparable to or less than the dipole-dipole interaction energy, polar molecules easily influence each other's trajectory and orientation, leading to complex dynamics. An externally applied field can manipulate the intermolecular interaction: for example, molecules can be made to collide (or not) on command, by varying the field strength with respect to the distance-dependent intermolecular dipole interactions. This mechanism represents a profoundly different type of control over collisions than resonant scattering controlled by a magnetic field. Additionally, the OH molecule possesses a sizable magnetic moment and is suitable for magnetic trapping, leaving the electric field free to control intermolecular interactions. Furthermore, with the existence of a cold, trapped sample, the small mass of OH radicals should aid a direct laser cooling effort through vibrational transitions around  $2.8 \mu\text{m}$ , as cycling through the lowest vibrational transition requires only three repumping lasers. Finally, we note practical, limited laser cooling along relatively radiatively closed electronically excited pathways is possible for OH.

A roadblock for cold molecular experiments is the need to develop effective approaches to detect, image, and characterize small samples of cold molecules once they are trapped. This is a prerequisite for exploring molecular condensates, coherent atom-molecule conversion, cold molecule collisions, and ultracold chemistry. For this purpose, an important feature of using OH radicals is ease of detection through laser-induced fluorescence (LIF). Resonance fluorescence has been developed as a highly sensitive technique for detecting small numbers of molecules. By counterpropagating a LIF laser beam along the molecular beam path, we can make definitive *in situ* observations of the molecular population, density, and velocity distribution at various positions within the

decelerator, leading to a clear picture of longitudinal phase-space evolution.

It is notably difficult to adapt the supersonic expansion technique that accommodates efficient production of cold, ground state free radicals via discharge or photolysis and still remain suitable for the Stark manipulation approach, which relies on the coupling of a near-collimated molecular beam into inhomogeneous electric fields. We utilize a high-voltage ( $\sim 3$  kV) discharge to create OH radicals. Figure 1 shows the experimental setup along with the detected OH signals along the beam path. Xenon (Xe) gas is bubbled through a small tank of distilled water with a backing pressure of 2.5 atm. The pulsed valve has a 0.5 mm diameter nozzle and is operated at a 5 Hz repetition rate, producing a supersonic beam with pulse widths of  $<100 \mu\text{s}$ . Two thin stainless steel disks act as discharging electrodes with electrons flowing against the expanding supersonic jet through the central 4 mm opening. Experimentally we find that operating the discharge voltage in a pulsed mode with a  $\sim 2 \mu\text{s}$  duration significantly reduces undesirable heating of the molecular beam. The measured mean velocity of the beam and the associated spread are  $375 \pm 60$  m/s, consistent with a near room temperature, Xe-seeded supersonic expansion. Another benefit of the short discharging pulse is that the production of OH molecules is well defined both in time ( $<2 \mu\text{s}$ ) and position ( $<2$  mm). Trace (a) in the lower panel of Fig. 1 shows a corresponding discharge light signal that defines the origin for all timing axes in the subsequent data figures throughout this Letter. State-selective fluorescence detection determines that greater than 93% of OH created is in the rotational and vibrational ground state ( $v = 0, J = 3/2$ ) of  $X^2\Pi_{3/2}$ . Within this state, the symmetrical “*f*” component is a weak-field seeking state with the  $|m_j| = 3/2$  components offering 3 times the Stark shift of the  $|m_j| = 1/2$ .

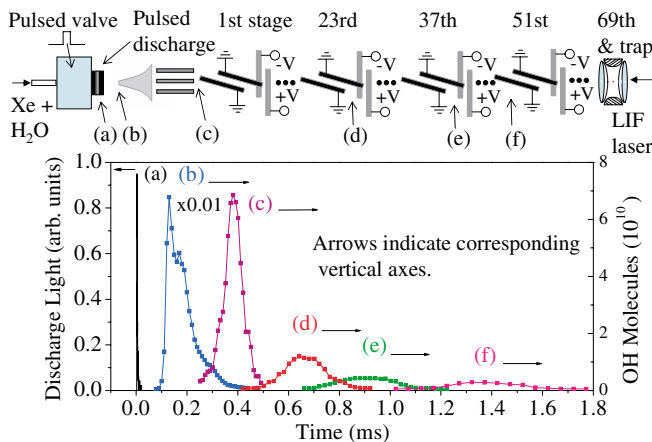


FIG. 1 (color). Upper panel: schematic of the Stark decelerator for free radical OH. Lower panel: (a) discharging light at nozzle; LIF signal, (b) before skimmer ( $\times 0.01$ ), (c) after hexapole, (d) after 23 stages, (e) after 37 stages, (f) before 51 stages.

After traversing a 1.5 mm aperture skimmer, which is charged ( $-300$  V) in order to deflect ions generated in the discharge, the molecular beam is focused into the Stark decelerator [7] by a short hexapole. The linear accelerator is formed by 69 pairs of 3.2 mm diameter rounded stainless steel rods with a center-to-center separation of 5.2 mm, allowing a  $2 \times 2$  mm<sup>2</sup> transverse acceptance area. Pairs of electrodes define individual slowing stages. Successive stages are separated by a center-to-center distance of 5.5 mm and are oriented alternately at  $90^\circ$  relative to each other in order to provide transverse guiding. At the end of the decelerator an electric quadrupole trap is located 14 mm from the last decelerator stage.

A frequency-doubled pulsed dye laser ( $\sim 10$  ns pulse duration) is tuned resonant with the  $A^2\Sigma^+(v = 1) \leftarrow X^2\Pi_{3/2}(v = 0)$  transition at 282 nm for fluorescence detection at 313 nm  $A^2\Sigma^+(v = 1) \rightarrow X^2\Pi_{3/2}(v = 1)$  (lifetime  $\tau = 750$  ns). The laser beam is introduced into the decelerator region through the 2 mm diameter apertures centered on the end caps of the quadrupole trap. The laser beam counterpropagates down the entire slower through the skimmer and into the valve region. The vacuum chamber has large solid-angle optical access for fluorescence collections along the molecular beam path. The sensitivity of the fluorescence measurement is enhanced by the favorable 72% branching ratio into the detection decay channel. To suppress scattered laser light, we inhibit the photomultiplier tube (PMT) during the excitation laser pulse and collect fluorescence signals only during the subsequent microsecond scale decay lifetime. The detected fluorescence signals are converted to the corresponding molecular numbers using carefully calibrated parameters such as laser intensity, photon detection efficiency, decay branching ratio, etc.

Following conventions used in linear accelerator physics (for a more detailed discussion, see Refs. [7,8]), we define a local spatial coordinate for a molecule located between two successive stages  $\phi = (z/2L)(360^\circ)$ , with  $z = 0$  defined at the center of the two stages when the voltages are switched. A molecule that is accelerated or decelerated has a different equilibrium position  $\phi_0$  than that of a constant speed molecule, which has  $\phi_0 = 0^\circ$ . The corresponding depth of the traveling potential well decreases as the magnitude of  $\phi_0$  increases. With  $\Delta\phi = \phi - \phi_0$  denoting spatial spread and  $\Delta\nu = \nu - \nu_0$  velocity spread around the synchronous molecules located at the equilibrium position of the moving trap, the following equations describe the overall phase-space evolution:  $(d^2\Delta\phi/dt^2) + (\pi W/mL^2)[\sin(\phi_0 + \Delta\phi) - \sin(\phi_0)] = 0$ ,  $\Delta\nu = (L/\pi)(d\Delta\phi/dt)$ . Here  $m$  is the molecular mass and  $W$  denotes the maximal energy loss (or gain) per stage.

To demonstrate the powerful capability of *in situ* detection of molecules within the decelerator for the study of phase-space manipulation, we select five representative regions for LIF signal collection as shown in Fig. 1: (b) before the skimmer, (c) between the hexapole and the first decelerator stage, (d) between the 23rd and 24th

stages, (e) between the 37th and 38th, and (f) between the 50th and 51st. Detection at regions (b) and (c), with the corresponding signals shown in the lower panel of Fig. 1, allows for optimization of OH production from the valve, discharge, and hexapole focusing. Experimentally we optimize the magnitude and duration of the applied hexapole voltage for a selected velocity class in order to provide transverse phase-space matching into the decelerator. Applying static voltage to the decelerator electrodes transversely guides the molecular beam. The LIF signals detected at (d), (e), and (f), such as those shown in Fig. 1, are obtained with  $\pm 12.5$  kV guiding voltages applied to all stages, resulting in a  $> 10\times$  signal enhancement. In all traces shown, the electric fields are switched off prior to molecular detection.

Given good spatial resolution in signal collection, the LIF signal, presented with respect to the time-of-flight through the selected detection region, reveals the longitudinal spatial and velocity distributions, which are input parameters for our model of the Stark manipulation process. We image a 2 mm long beam section located between two successive pairs of electrodes onto the PMT, with a magnification of 2.7 to aid spatial filtering. Figure 2 shows time-of-flight LIF signals observed after 14 stages of inhomogeneous electric fields switched with precise timing, followed by nine additional stages of static transverse guiding. Figure 2(a) depicts the transversely guided molecular packet. With the electric fields having the same magnitude and configuration as in the static guiding case except that the voltages are now switched at a frequency matching  $\nu/2L$ , bunching of molecules is demonstrated in Fig. 2(b). Here  $\nu$  is the mean velocity of the molecular packet (375 m/s) and  $L$  is the distance between the successive, orthogonally oriented stages. The switching effectively creates traveling potential wells in which molecules are trapped, producing the central bunched peak marked by the arrow in the figure. Other peaks and valleys visible in trace (b) are created by phase-space

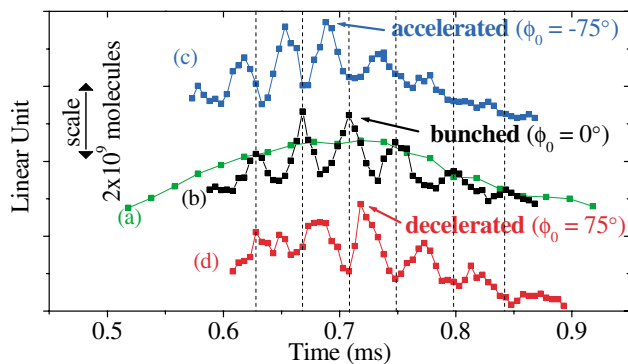


FIG. 2 (color). (a) Transverse guiding, (b) bunching, (c) deceleration, and (d) acceleration of OH after 14 stages of Stark slowing followed by 9 additional stages of transverse guiding. For the sake of clarity, the deceleration and acceleration data are shifted vertically. The peaks marked by arrows represent molecules trapped in the moving potential wells.

open trajectories of untrapped molecules. By chirping the switching frequency, the molecules' speed can be increased to 421 m/s [Fig. 2(c)] or decreased to 323 m/s [Fig. 2(d)], depending on the sign of the frequency chirp; this results in the central molecular peak arriving earlier (when accelerated) or later (when slowed) in time, relative to the bunched peak. Clearly, the *in situ* detection capability has allowed us to simultaneously monitor, stage by stage, the trapped and untrapped molecular dynamics, showing temporal transportation of the untrapped molecules as theoretically investigated in [12]. Our numerical simulations account for these dynamics in a detailed manner.

Numerical simulations are derived from a detailed understanding of the Stark slower and OH molecules. From the measured geometrical and electrical properties (sizes, distances, and applied voltages), an electric field map of the slower is constructed, which when coupled with understanding of the OH energy structure (including both  $|m_j| = 3/2$  and  $1/2$  levels, with a mixing ratio of 3:1 resulting from the initial hexapole selection), gives complete information on the forces experienced by OH molecules within the decelerator region. From the static guiding data the initial velocity distribution of the molecules is calculated, allowing the generation of a sample of the initial molecular longitudinal phase space. This 1D phase-space distribution is then propagated through the Stark manipulation process resulting in a phase-space distribution similar to those of Figs. 3(c) and 3(d). Next, the distribution is spatially integrated to produce a time-of-flight spectra that is compared directly to the experimental data as shown in Figs. 3(a) and 3(b).

The LIF experimental configuration is particularly suitable to visualize effects described by the equations given above. Molecular packets can be monitored at

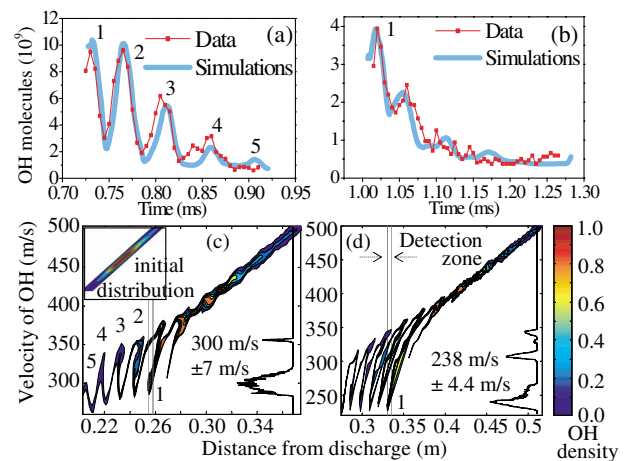


FIG. 3 (color). Measured time-of-flight distribution at (a) 23 stages and (b) 37 stages (22 and 36 stages of deceleration, respectively, followed by guidance for one stage). Also shown are instantaneous pictures of phase space distributions of OH after (c) 22 and (d) 36 stages of deceleration. In both (a) and (b), data points are red squares and theory thick blue lines.

various stages immediately following the deceleration process, or after additional transversely guided free flight, to provide phase-space information. Figures 3(a) and 3(b) show two cases where the LIF detections are made after 22 and 36 stages of deceleration at  $\phi_0 = 75^\circ$ , followed by one stage of free flight. Corresponding numerical simulations are shown as solid lines for both panels. The simulations confirm that the largest peak at 1.02 ms in Fig. 3(b) is associated with the  $|m_j| = 3/2$  state and the second peak at 1.05 ms for  $|m_j| = 1/2$ . The simulation results are obtained from the phase-space distribution contours shown in the corresponding panels (c) and (d) of Fig. 3, which also includes a color-coded scale bar for normalized molecular numbers. As shown in the inset of Fig. 3(c), the initial phase-space distribution ( $v : 375 \pm 60$  m/s;  $z : 0.13 \pm 0.02$  m) at the input of the decelerator is a result of molecular free flight from the nozzle. Simulations are carried out with no free parameters except a global scaling factor. The thickness of the simulation curves signifies the measurement uncertainty of the geometrical dimensions of the entire decelerator ( $\pm 1$  mm over 40 cm), without taking into account other real-time fluctuations in switch timing, laser intensity, and molecular numbers. It is most likely these uncertainties along with focusing effects perpendicular to the longitudinal direction account for the observed small discrepancies in Figs. 3(c) and 3(d). Nevertheless, the agreement between simulations and experimental data is excellent.

In the first case of 22 stages of deceleration, there are five distinct spatially separated distributions in Fig. 3(c), labeled, respectively, as 1, 2, 3, 4, and 5. These distributions fly through the detection zone indicated by vertical blue lines, leading to the observed LIF signals shown in Fig. 3(a). It is clear from Fig. 3(c) that packet one represents the trapped molecules that have migrated from the original phase-space distribution. The projected velocity distribution associated with one is also shown near the right vertical axis, indicating a 7 m/s velocity spread. When the deceleration process is carried to the 36th stage, the mean velocity of the molecular packet is further reduced, along with additional rotation of the phase-space distribution, as shown in Fig. 3(d), leading to a narrower velocity spread of 4.4 m/s. Part of the reduction of the velocity width is attributed to the departure of untrapped molecules from the packet, as shown in both experimental data and simulations.

Finally, as shown in Fig. 4, when the deceleration process is continued to the 50th stage, the slow molecular packet (red circles) ( $\phi_0 = 75^\circ$ ) has now been completely decelerated out of the transversely guided molecular distribution (green diamonds). The phase-stable molecular packet has been decelerated to 140 m/s with a velocity spread of 2.7 m/s, corresponding to a longitudinal temperature of 15 mK. Simulations again confirm the position and width of the measured packet, which is now solely attributed to the  $|m_j| = 3/2$  state. The bunched peak (black squares) ( $\phi_0 = 0^\circ$ ) appears 0.3 ms earlier than

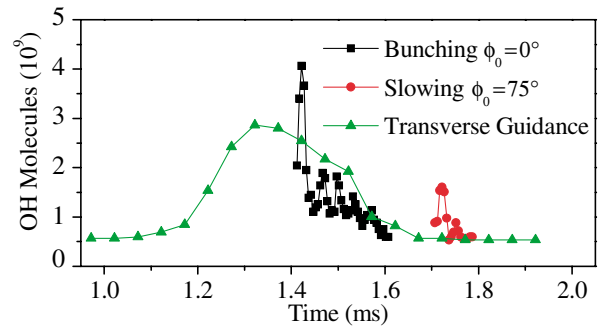


FIG. 4 (color). OH molecules after 50 stages of transverse guidance (green diamonds), bunching (black squares), and deceleration (red circles). We note that experimental conditions fluctuate from day to day resulting in molecular number variations.

the slowed packet in the measured time-of-flight distribution. After the slowing process is continued through the entire decelerator, we expect to trap similar numbers of molecules at equivalent temperatures.

In conclusion, we have presented clear evidence for the first time of longitudinal phase-space manipulations of free radical molecules, demonstrating bunching, slowing, and acceleration of a ground rovibrational state of OH. The experimental approach presented here has led to an excellent understanding of the associated physical processes and will have a major impact on future cold molecule work where *in situ* detections can be critical for observations of cooling and trapping dynamics.

We thank J. Bohn, E. Cornell, and D. Nesbitt for useful discussions and A. Pattee, M. Silva, T. van Leeuwen, and H. Bethlem for technical help. This research is supported by NSF, NIST, and the Keck Foundation. J. R. B. and H. J. L. acknowledge support from NRC.

\*Fritz-Haber-Institut der Max-Planck-Gesellschaft, Faradayweg 4-6, Berlin D-14195, Germany.

†Email address: ye@jila.colorado.edu

- [1] E. A. Cornell and C. E. Wieman, *Rev. Mod. Phys.* **74**, 875 (2002); Wolfgang Ketterle, *ibid.* **74**, 1131 (2002).
- [2] T. Takekoshi, B. M. Patterson, and R. J. Knize, *Phys. Rev. Lett.* **81**, 5105 (1998).
- [3] J. D. Weinstein *et al.*, *Nature (London)* **395**, 148 (1998).
- [4] H. L. Bethlem *et al.*, *Nature (London)* **406**, 491 (2000).
- [5] A. Fioretti *et al.*, *Phys. Rev. Lett.*, **80**, 4402 (1998); R. Wynar *et al.*, *Science* **287**, 1016 (2000).
- [6] E. A. Donley *et al.*, *Nature (London)* **417**, 529 (2002).
- [7] H. L. Bethlem *et al.*, *Phys. Rev. Lett.* **84**, 5744 (2000); **83**, 1558 (1999).
- [8] H. L. Bethlem *et al.*, *Phys. Rev. A* **65**, 53416 (2002).
- [9] M. Wardle and F. Yusef-Zadeh, *Science* **296**, 2350 (2002).
- [10] X. H. Liu *et al.*, *Science* **289**, 1536 (2000).
- [11] A. V. Avdeenkov and J. L. Bohn, *Phys. Rev. Lett.* **90**, 043006 (2003).
- [12] G. J. Dong, W. P. Lu, and P. F. Barker, *J. Chem. Phys.* **118**, 1729 (2003).